Pergamon

Journal of Structural Geology, Vol. 20, No. 12, pp. 1673 to 1689, 1998

PII: S0191-8141(98)00080-7
0191-8141/98/$ - see front matter

Fracture initiation, growth and effect on stress field: a numerical investigation

STEPHEN D. McKINNON*

Itasca Consulting Group, Inc., 708 South 3rd St, Suite 310, Minneapolis, Minnesota 55415, U.S.A.

and

IVAN GARRIDO de la BARRA

Almirante Zegers 672-D, Providencia, Santiago, Chile

(*Received* 20 *January* 1997; *accepted in revised form* 2 *July* 1998)

Abstract—A numerical investigation was made of the relationships between fracture initiation, growth, stress field and boundary conditions. Two-dimensional plane strain continuum models were used in which fractures appeared as zones of strain localization developed through application of a strain softening Mohr–Coulomb constitutive model. R and R' fractures developed first, followed by Y fractures at larger strains. The models showed that equal development of conjugate R and R' fractures is easily changed to favor one or the other set by minor variations in model initial conditions. Strength loss in fractures caused stress field rotations in regions bounded by fractures, altering the orientation of subsequent fractures. The amount and sense of stress field rotation is dependent on the strength loss during displacement on the fractures, the orientation of fractures, and on the boundary conditions. Y oriented fractures could be explained on the basis of a Mohr–Coulomb failure criterion provided that stress field rotation is accounted for. Monitoring of fracture slip activity showed that, under conditions of constant boundary velocity, slip was discontinuous in time, alternating on fractures throughout the model.

INTRODUCTION

There are differing reports about the sequence of formation of the Riedel family of fractures. Reproducing Riedel's classic clay cake experiment (Riedel, 1929), Tchalenko (1970) observed simultaneous formation of conjugate R and R' fractures followed by P fractures linking the Riedel shears. Y fractures, which occur parallel to the direction of shearing, were observed to form at large displacement. In a series of confined wrench experiments using limestone, Bartlett *et al.* (1981) observed simultaneous formation of P fractures with the R and R' fractures, followed by Y oriented fractures at larger displacement. Naylor *et al.* (1986) attributed the orientation of P shear fractures to the rotation of the initial stress field caused by primary Riedel fractures. Using large three-dimensional numerical models of wrenching, Braun (1994) reproduced all Riedel shear fractures. In these numerical experiments a zone of diffuse Y shears developed first, followed by conventional R and R' shears. One can conclude that there is still debate over the sequence and mechanism(s) responsible for the formation of these fractures. It appears that the sequence is related to the complex interaction of the stress field and fractures which cannot easily be explained by conventional small strain failure criteria. It was the objective of this investigation to examine more closely the relationships between fracture growth and stress field orientation.

Theoretical studies of the initiation of strain localization in brittle material have been made by Rudnicki and Rice (1975), and Vermeer (1982), including their effects on the stress field. More geologically oriented studies of fracturing in rock (Hobbs and Ord, 1989; Cundall, 1990; Olson and Pollard, 1991) have involved the use of numerical models in order to capture more complex boundary and initial conditions. A numerical approach was selected for this study as numerical models enable detailed information to be extracted regarding both stresses and displacements. This would not have been possible with analytical or analogue models. The experiment began with initially intact material and fracture initiation and growth was induced by controlled displacement of the model boundaries. By developing fractures (shear bands in our continuum models) from initially intact material, potential compatibility problems of having to make a priori assumptions about the stress field around fractures were avoided. Fracture growth, displacement, and stress field orientation would always be linked through the material constitutive model. In this modeling, issues of fracture initiation, growth, orientation, effect of boundary conditions, effect of fractures on stress field, effect of fracture strength, and block kinematics were addressed.

*Author for correspondence. e-mail: sm@itascacg.com.

A common terminology (Sylvester, 1988) for brittle shear fractures in rock is shown in Fig. 1. Riedel fractures, R and R', form a conjugate set about the major principal stress direction. Tension fractures, T, form in the direction of major principal stress, and P fractures form symmetrically to the R fractures with respect to the shear direction. Y fractures are those which are parallel to the direction of applied shear displacement. All of these fracture types have been observed in nature (Tchalenko and Ambraseys, 1970; Gammond, 1983) and as reported by Bartlett *et al.* (1981), they have all been reproduced in various laboratory tests.

The orientation of R and R' fractures can be deduced from the Mohr circle. For a rock with strength defined by cohesion c and friction angle ϕ, fracture occurs on planes oriented at $\pm(45^\circ - \phi/2)$ from σ_1 as shown in Fig. 1. Depending on the amount of confining pressure, σ_3, tension fractures T may occur parallel to the σ_1 direction.

Using plasticity theory, Vermeer (1990) has shown that in an elastic/perfectly plastic material, shear bands may occur over a range of angles θ from the σ_1 direction:

$$45^\circ + \psi/2 < \theta < 45^\circ + \phi/2 \qquad (1)$$

where ψ is the angle of dilation of the material during shearing. Shear bands or fractures, therefore, need not occur at only one specific angle, but could occur over a range of angles. On the basis of small strain Mohr–Coulomb theory, however, it is not possible to explain the formation of primary P or Y fractures.

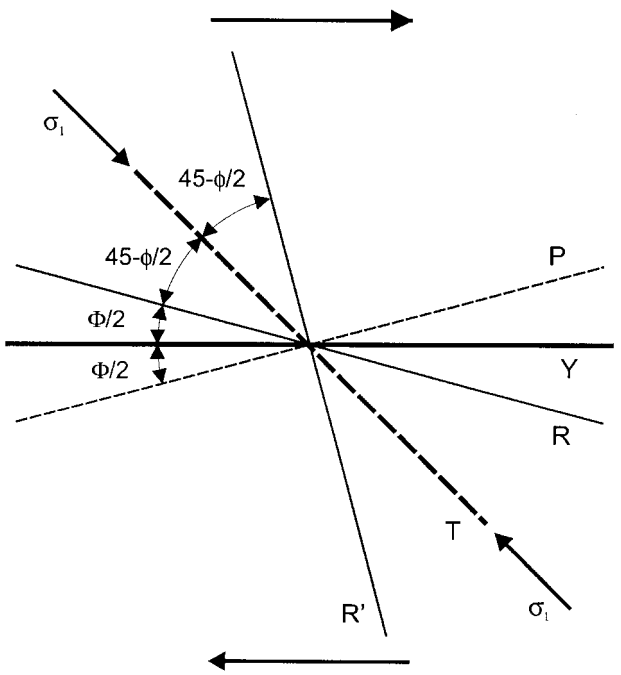

Fig. 1. Fractures associated with the Riedel model showing typical orientation relative to the major principal stress and direction of shearing.

NUMERICAL MODELING CONSIDERATIONS

As with any experiment, certain decisions about how to build the models were made. For numerical models, choices were made about the method (finite difference, boundary element, etc.), size of model, boundary conditions, initial stress field, material properties and constitutive model. Since any one of these can affect the outcome of a numerical experiment, a brief description of the relevant considerations is provided.

Modeling method and model construction

Following the work of Cundall (1989, 1990), and Hobbs and Ord (1989), the two-dimensional stress analysis code FLAC (Itasca Consulting Group Inc., 1995) was used to model primary fracture initiation and growth. The finite difference scheme used in this code implements the full equations of motion, including inertial effects, updating the gridpoint geometry incrementally in a time marching fashion. Damping is used to reduce out-of-balance forces enabling the material to maintain quasi-static equilibrium. This type of solution scheme is ideally suited to tracking complex material behavior through large strains. A strain softening constitutive law was used in most of the models although similar results were obtained using only an elastic/perfectly plastic law. A large strain formulation was also used to provide a 'memory' in the material of where fractures were located. Using a large strain formulation, grid geometry is updated according to material deformation, thereby tracking deformation history. In small strain formulations, the initial grid geometry is preserved. Strength loss in the softening law was applied to cohesion only, with complete loss after a post-peak strain of 0.05.

Grid considerations

Each model comprised a grid of quadrilateral finite difference zones. Development of shear bands in continuum models occurs through yielding of individual zones in the grid. With a decreasing number of zones, resolution of shear bands reduces and distinct bands do not occur. Grid effects are also more pronounced if fewer zones are used. Because of these effects, models consisting of between 5000 and 7000 zones were used. It was found that models with approximately one quarter of this size were not large enough to resolve shear bands whereas larger models simply took longer to run.

With a strain-softening law, yielding zones become weaker with increasing strain. Since strain increases as the width of the localization decreases, there is a biasing of the shear bands towards an alignment parallel to the grid axes as this results in shear bands of one zone width (the minimum possible), maximizing strain.

This is a weakness of grid-based continuum codes applied to modeling of strain localizations. Certain measures were taken to reduce this effect. These included rotation of the entire grid such that one grid axis became parallel to the initial major principal stress direction. In this way the initiation of either of the conjugate Riedel shears would be equally biased. Another method used was to randomly relocate grid-points such that the grid did not conform to a regular square configuration. In some cases, both techniques were used together, i.e. a rotated randomized grid. Both methods resulted in a reduction of grid dependent effects, but the effect could not be completely eliminated. More complex schemes have been suggested in the literature, e.g. Bazant (1992), but these modifications were beyond the scope of this work.

In reality, rock is rarely homogeneous on any scale, and fractures would be expected to initiate at local points of weakness or stress concentration. To simulate this effect, and to avoid triggering fractures caused by characteristics of the grid, the Young's modulus of each zone was randomly varied. Modulus values were chosen from a triangular distribution with a maximum deviation of $\pm 20\%$ of the mean value. There was no spatial correlation between modulus values. The mean Young's modulus used in all models was 30 GPa and Poisson's ratio was constant at 0.2. At the start of the simulations, stresses in each zone were identical, but as deformation took place, those zones with higher modulus became more highly stressed and acted as random trigger points for yielding. While the effects of using different modulus variations were not explicitly investigated, experience with other models in which this effect was examined led to the belief that the results would be unaffected, provided the modulus variation was relatively small.

Boundary conditions

Boundary displacements were controlled to produce conditions corresponding to various combinations of simple shear and pure shear. Using the common assumption of zero volumetric strain during deformation, the definition of pure shear is unambiguous. In two dimensions, compression along one axis is compensated by lateral extension. There are, however, two commonly used boundary conditions for simple shear. In geological applications, strain is a primary quantity and the deformation matrix definition of simple shear leads to purely lateral particle displacement. In geotechnical testing (see Atkinson and Bransby, 1978, for example), apparatus is used that shears samples under constant confining pressure and permits vertical displacement to take place. These two types of deformation are referred to as confined (Fig. 2a) and unconfined (Fig. 2b) simple shear, respectively. Each was found to have different effects on fracture development.

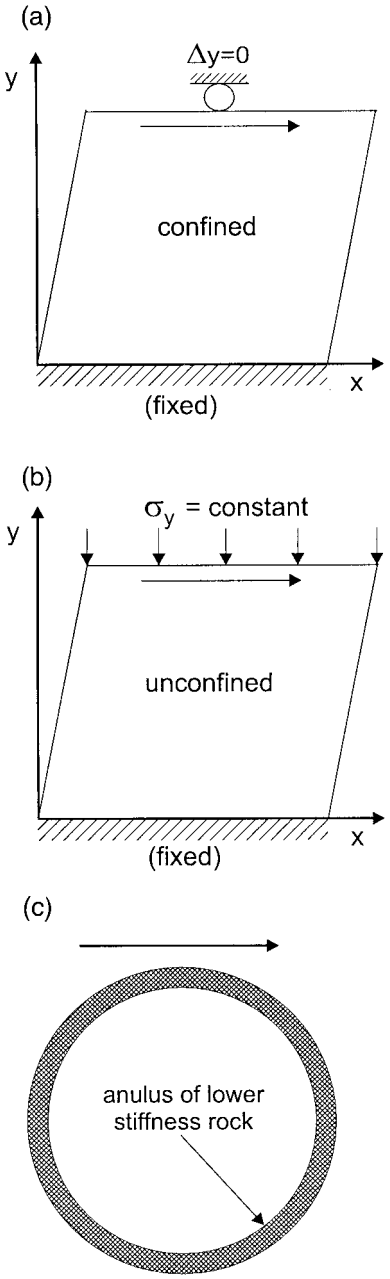

Fig. 2. Boundary conditions for different types of models used. (a) Confined simple shear; (b) unconfined simple shear; and (c) circular model with soft annulus deformed in combinations of simple and pure shear.

Both boundary conditions have analytical conveniences, but geologically, they are rather severe. It would be expected that resistance to deformation would be neither zero nor constant, but would increase with deformation as a result of interaction with surrounding material. A third type of boundary condition corresponding to this behavior was also used (Fig. 2c).

Initial state of stress

The initial state of stress in the models was set at the elastic strength limit in order that all computational effort would be devoted to following the fail-

ure process from initial yield, eliminating unnecessary tracking of elastic deformation. The initial state of stress was also specified to be entirely compressive since we wished to study fracture development according to a shear failure criterion and avoid generation of tensile stresses.

If an undeformed elastic block is subjected to simple shear it will develop equal magnitude compressive and tensile stresses inclined at 45° to the shear direction. This same state of stress can be initialized in an undeformed block and kept in equilibrium by appropriate boundary tractions. By adjusting the magnitude of the internal stresses and the boundary tractions, the stress field in the model can be set at the material yield point with all normal stress components compressive. By specifying the strength of the material in terms of a Mohr–Coulomb cohesion c and friction angle ϕ, the principal stress magnitudes at the yield point can be calculated. In these models, the material strength was set at $c = 4.3$ MPa and $\phi = 55°$. The initial mean stress was 25 MPa. Different angular relations between fractures would occur for other strength values, but the general observations would remain unchanged.

The orientation of the stress field in the model at the yield point is critical to the orientation of fractures that will be produced. In simple shear, the stress field is oriented with major principal axis at 45° to the shear direction. As increasing amounts of pure shear are added, the major principal axis rotates towards the direction of pure shear compression. To define the relative amounts of pure and simple shear for cases of oblique compression, the arctangent of the ratio of lateral simple shear displacement δ_x to pure shear displacement δ_y, which we refer to as the convergence angle α, was used (Fig. 3a). Using this definition for oblique compression, the orientation of the major principal stress ψ in an elastic material can be calculated as:

$$\psi = \frac{\pi}{2} - \tfrac{1}{2}\tan^{-1}\frac{1}{2\tan\alpha} \qquad (2)$$

where ψ is measured clockwise from the plane of simple shear displacement to the direction of the major principal stress (Fig. 3b). This equation was used to establish the orientation of the initial stress field in the numerical models. Simple numerical experimentation showed that significantly different fracture patterns could result if this initial stress field orientation was not used. These more complex loading paths will not be described here.

EN ÉCHELON FRACTURES AND THREE-DIMENSIONAL CONSIDERATIONS

Many of the experiments that were used to study Riedel shear fractures are inherently three-dimensional. The clay cake experiments of Riedel (1929) and Tchalenko (1970), the limestone wrench experiments of

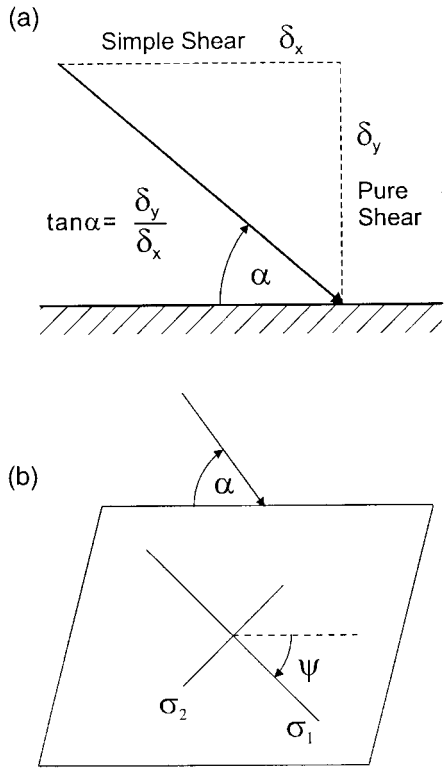

Fig. 3. (a) Definition used for boundary displacement when combining simple and pure shear; and (b) the relation of boundary displacement with stress field orientation in plane strain.

Bartlett *et al.* (1981), and the numerical experiments of Braun (1994), all produced flower-like structures with curved fracture surfaces. Since it would be preferable to use two-dimensional models for this study, how can their use be justified in view of the three-dimensionality of the problem? Firstly, attention is restricted to small post-failure strains. Kinematic effects, such as finite block rotation, are undoubtedly important at large strains but this will not be the focus.

Next, using a simple three-dimensional model of an elastic block with an underlying basal transcurrent shear discontinuity it can be shown that the stress field near the surface, above the discontinuity, is identical to that produced by simple shear boundary conditions in two-dimensions. Although a plane stress model would better approximate this region, no difference was found between plane strain and plane stress model results. Finally, the results also may be of interest from a purely two-dimensional point of view for situations in which the plane strain or plane stress assumption is valid.

An important limitation of two-dimensional models is their inability to reproduce fracture patterns that result from three-dimensional mechanisms. In our review of fracture formation, it appeared that there are many examples in which *P* fractures are considered to be secondary fractures that form in response to finite strain effects (Tchalenko, 1970; Tchalenko and Ambraseys, 1970; Gamond, 1983). Based on results from the three-dimensional elastic model described

above, the en échelon formation of fractures can be attributed to the shape of the three-dimensional stress field forming above the basal transcurrent fault. R and R' fractures developing within a band above the basal fault are speculated to form the en échelon pattern. This pattern cannot be reproduced in two-dimensional models, and therefore, the secondary P fractures linking the primary fractures can also not be formed. We therefore restricted our attention to primary fracture formation, or the initial fractures, which do not undergo large strain.

NUMERICAL MODELING OF PRIMARY SHEAR FRACTURES

Confined simple shear

Shear displacement of the top boundary of the models (Fig. 2a), was set at 1×10^{-5} units per step in a right-lateral sense. For the dimensions of the model used, this corresponds to a plastic shear strain of 1.25×10^{-7} per step. Since absolute strain is not of direct importance, as we are interested in the sequence of fracture formation, reference will be made to step number. Displacements on the side boundaries were controlled such that gridpoint velocities on opposite boundaries were linked. This type of boundary condition makes the material response periodic in that the left side of the model is numerically attached to the right hand side.

Figure 4(a) shows the location of 'fractures' in the model after 20,000 steps. In all cases, 'fractures' are localized concentrations of shear strain. Throughout the paper, numerically generated fractures are shown as contours of plastic shear strain. Based on the angular orientation of these fractures relative to the initial stress field, they correspond to R, R' and Y fractures. Formation of R fractures occurred relatively early in the simulation, within the first 500 steps. After approximately 1000 steps, the first R' fracture appeared. In the models of confined simple shear, only one R' fracture occurred, as shown in Fig. 4(a). With continued deformation, shear strain selectively concentrated in a smaller number of fractures. At approximately 10,000 steps, the first development of Y fractures appeared. Shear strain activity slowly progressed from the R and R' fractures to the Y fractures.

At any instant in time throughout the simulation, shear strain activity was only seen on a small number of fractures. Activity on any particular fracture therefore appeared periodic. Over longer periods of time, this alternating activity resulted in distributed strain. Detailed analysis of unbalanced force at gridpoints as a function of time in this and other models (analogous to seismic events) showed a power law distribution of the same form as the Gutenberg–Richter law of seismicity. This indicated that over time, shear strain in the models was distributed over a wide range of scales. Coherent slip on the fractures was similar to periodic events of large magnitude.

After 20,000 steps, shear strain activity was concentrated almost exclusively on Y fractures. Figure 4(b) shows a plot of shear strain rate corresponding to the cumulative fracture pattern in Fig. 4(a). Kinematically, neither R nor R' fractures are oriented favorably to accommodate large deformations, whereas Y fractures are. Velocity vectors in a small region of the model centered over a fracture (Fig. 4c) show that the direction of material transport after Y fracture formation is generally parallel to the direction of applied shear deformation, and not parallel to previously formed Riedel shear fractures.

The stress field associated with the same small window of the model is shown by the pattern of stress tensors (Fig. 4d). In this, and all other plots showing stress tensors, axis lengths are proportional to principal stress magnitude. Within the area of the localization, stress magnitudes are much lower than outside and the orientation of the stress field also differs. The stress field outside the localization is relatively uniform, but throughout the simulation, there was a progressive counterclockwise rotation of principal axes. At the strain level shown in Fig. 4, the total rotation varied between 10° and 20°, and up to 30° close to fracture tips. Since the initial stress field was inclined at 45° to the horizontal, equation (1) shows that the orientations of new R fractures formed relative to this rotated stress field are compatible with the Y orientation. Although we did not see development of new R fractures progressing from the initial orientation through the Y orientation, it appears that the R, R' and Y fractures can be predicted on the basis of conventional Mohr–Coulomb behavior, provided the rotation of the stress field is accounted for.

To elaborate on how fractures affect the stress field orientation, a numerical experiment using a single elastic zone was made to show how stress field orientation would change if no fracturing occurred. With a positive simple shear displacement, the orientation of the major principal stress rotated progressively in a *clockwise* direction. In the models described above, R fractures caused a *counterclockwise* rotation of much larger magnitude. Even though the stress field underwent considerable rotation because of fracture formation, there was still a reasonable degree of coherency in the orientation of σ_1 outside of the shear bands, as shown in Fig. 4(d).

Unconfined simple shear

These models were identical to those discussed in the previous section, except that the top boundary condition was changed to a constant normal stress (Fig. 2b), enabling dilation to occur in the vertical direction. During the early stages of deformation, frac-

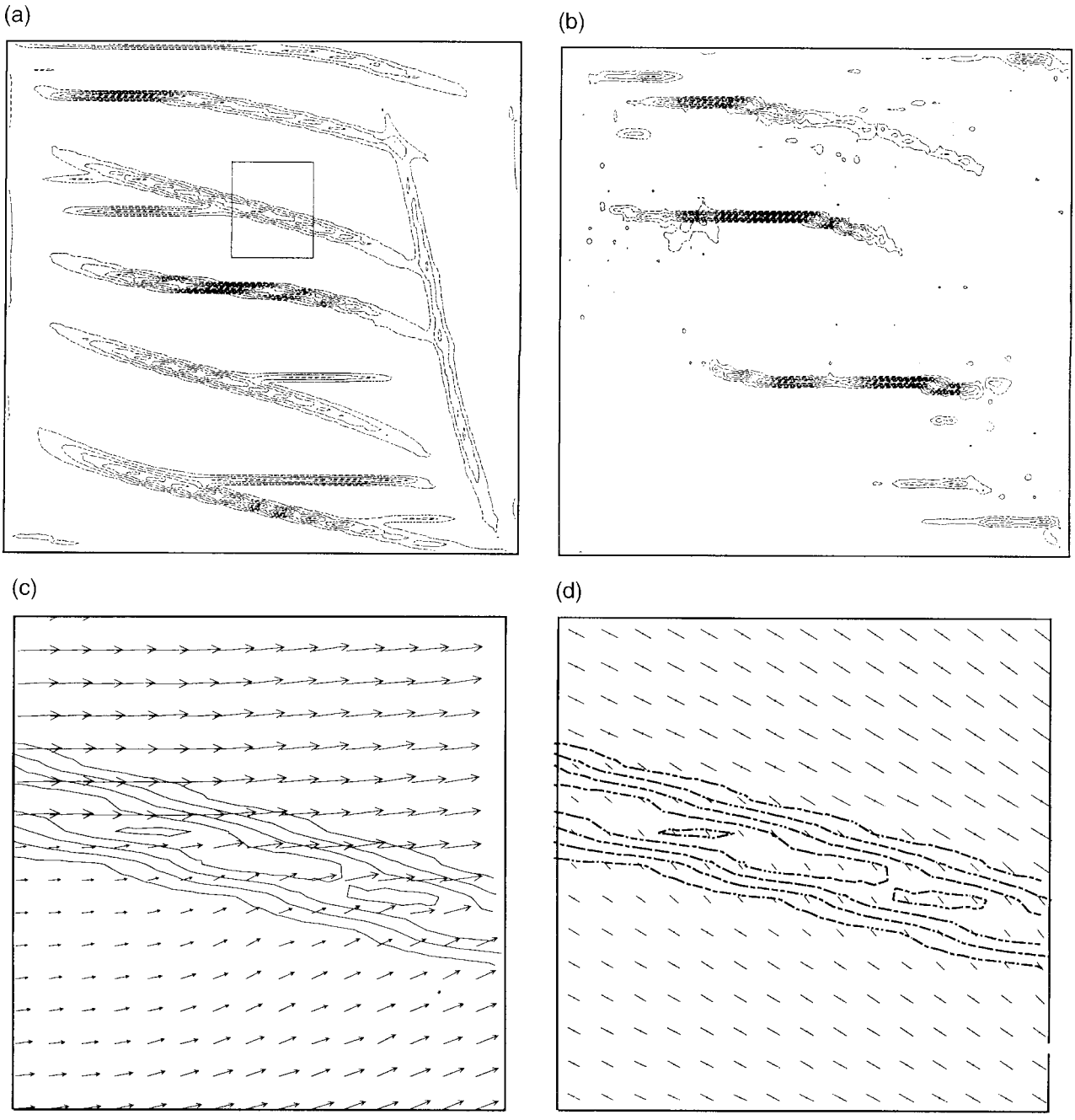

Fig. 4. (a) Contours of shear strain showing fracture pattern resulting from right-lateral simple shear; (b) snapshot of shear strain rate showing instantaneous shear activity; (c) detail of model [see box in (a)] showing velocity vectors and shear localization; and (d) same detail showing stress field.

ture evolution followed one of two paths. In some models, R' fractures quickly dominated over R fractures, and all subsequent fracture deformation was controlled by the geometry of the R' fractures. The second mode of fracture development initially followed the same trends as the confined models, with predominantly R fracture formation. However, at larger strain levels, R' fractures started to form, and subsequently, shear displacement occurred predominantly on R' fractures. In all of the unconfined models, R' fracture deformation dominated the final behavior. While the reason for either R or R' fractures dominating the initial behavior was not explored, R' fractures appeared more likely to occur if a grid with constant, as opposed to randomized, modulus values was used. It is possible, therefore, that grid effects were triggering the initially strong R' development in those models.

R' fractures have an important effect on the kinematics of the fractured system. Figure 5(a) shows a sketch of a typical fracture pattern from these models. R' fractures defined blocks which moved in a toppling mode over a lower R fracture. The lower R fracture formed because the bottom boundary of the model was fixed. Gridpoint velocities indicated that the block

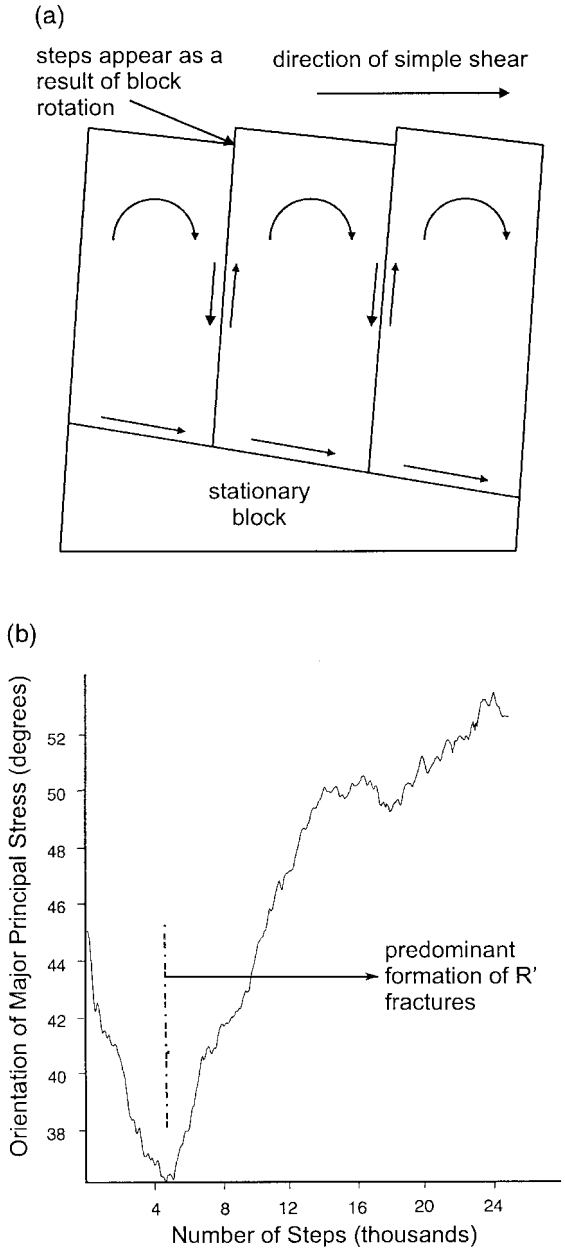

Fig. 5. (a) Typical fracture pattern resulting from unconfined right-lateral simple shear showing sense of block movement. (b) Orientation of major principal stress axis which rotates in a clockwise direction during R fracture formation but counterclockwise when displacement on R' fractures dominates.

below the lower R fracture was effectively stationary and deformation of this system involved shearing of the top part of the model over the lower block. Arrows in the sketch indicate relative motion.

Figure 5(b) shows how the average orientation of σ_1 changed during one simulation. Clockwise rotations from the initial orientation are positive. During the early stages of the simulation, σ_1 rotated counterclockwise, consistent with the formation of R fractures. However, at a later point there was a reversal of rotation to a clockwise direction, which corresponded to the initiation of R' growth in the model. This sense of rotation was consistent with the kinematic rotation of the blocks defined by R' fractures. The final dominance of R' shear bands and the reversal of the direction of stress field rotation was a result of the effect of boundary conditions. The periodic lateral boundary condition provided increasing kinematic resistance to continued R fracture displacement such that failure in the R' orientation was more favorable. We refer to this phenomenon as kinematic hardening, as it is a form of material strength increase that results from interaction of fractures with restraining boundaries. The importance of boundary conditions will be examined in greater detail later.

Simple shear with variable stiffness boundary constraint

The third type of boundary condition used for simple shear resulted in increasing resistance to fracture deformation at the boundary of the model. A circular grid model was used (Fig. 2c). Material properties for the interior region of these models were the same as in the square grid models and the surrounding annulus had a Young's modulus one-tenth that of the interior. A strain softening constitutive model was used for the interior region, whereas the annulus was elastic/perfectly plastic. Deformation of the system was controlled by specifying the velocity of gridpoints along the outer boundary of the model.

In these models, opposite sides of fractures extending to the edge of the interior region could displace relative to each other by indenting into the softer annulus. Resistance to indentation increased with increasing indentation. This type of boundary has some of the attributes of both the confined and unconfined models and is probably more realistic geologically in that lateral resistance is neither rigid nor absent.

Figure 6 summarizes the main features and results of two simple shear models. The difference between the two models was only in the form of the grid. In one model (Fig. 6a) gridpoint locations were randomized and the grid was rotated by 45° counterclockwise such that one grid axis was aligned with the initial major principal stress direction. This configuration would not bias the initial formation of either R or R' fractures. The model shown in Fig. 6(b) has some biasing in that the grid was rotated by 30° counterclockwise and was not randomly distorted. The latter grid favors formation of R' fractures since the R' orientation is more closely aligned than the R orientation with the 'channels' formed by the grid. These two simulations show sensitivity to initial conditions on the formation of R or R' fractures. While this is purely a numerical effect in our models, the same might occur in nature as a result of anisotropic rock strength or fabric.

Both R and R' fractures formed in the unbiased grid (Fig. 6c). The initial development of fractures was exclusively in the R orientation, with R' fractures

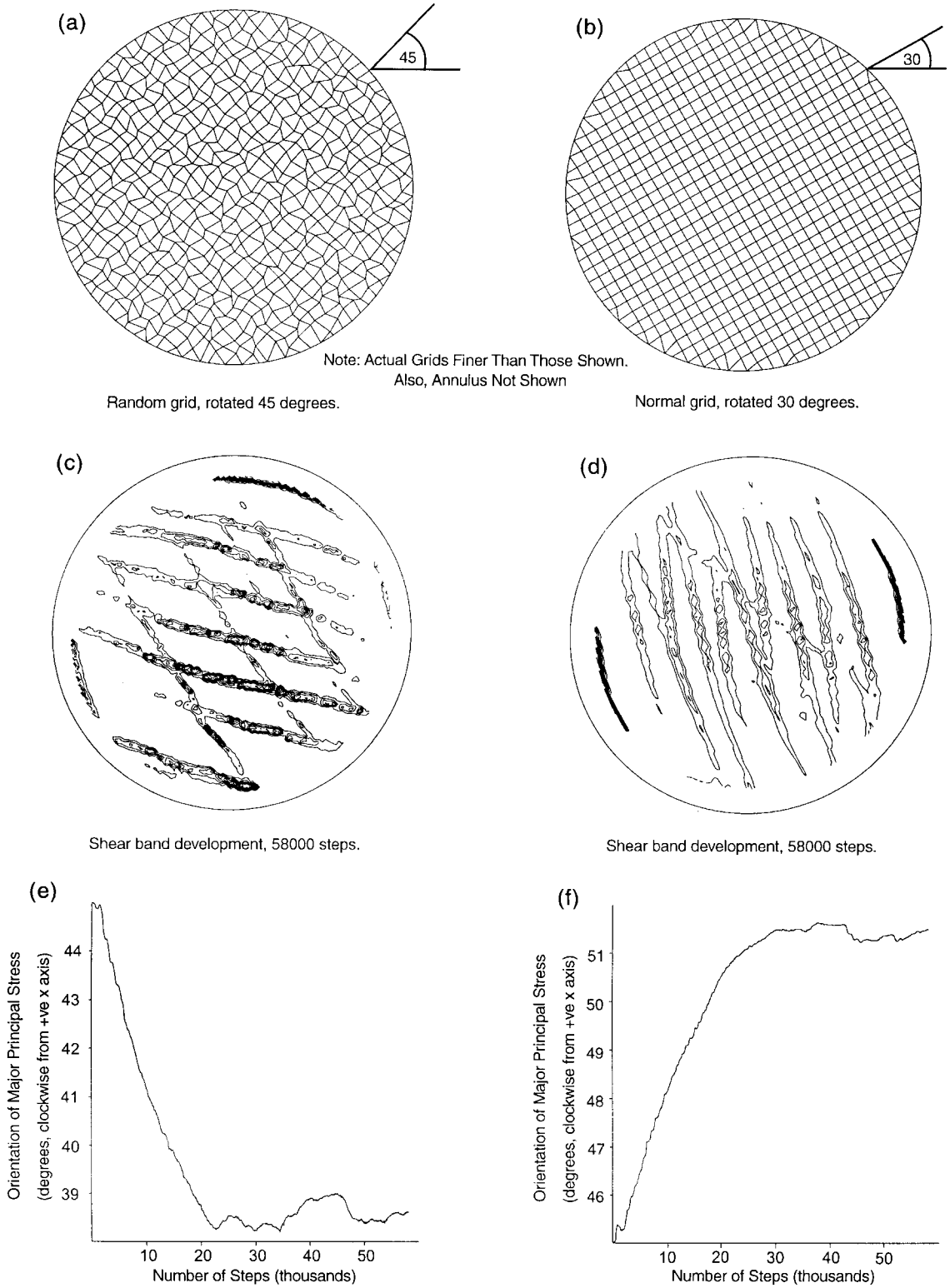

Fig. 6. Two examples of simple shear illustrating how small variations in initial conditions (grid effects) can lead to different fracture patterns. (a) and (b) show views of the grids, (c) and (d) show the corresponding fracture patterns, (e) and (f) show the average orientation of major principal stress in the models with displacement.

forming later in the simulation. R fractures remained as the most well developed set to the end of the simulation. Figure 6(e) shows the orientation of σ_1 against the number of steps in the simulation. There was a gradual counterclockwise rotation of σ_1 during the formation of R fractures until approximately 22,000 steps, at which time the rate of rotation stabilized, corresponding to the initiation of R' fractures.

The orientation of R fractures falls within the range defined by equation (1), but the R' fractures were

oriented at a smaller angle to the initial stress field than would be predicted by equation (1). This is as a result of the later formation of R' fractures in a stress field rotated counterclockwise by earlier formation of R fractures.

The results of the 'biased grid' model (Fig. 6b), showed a completely different fracture pattern for the same amount of boundary deformation. In this model, R' fractures dominated the evolution until relatively late stages of the simulation. R' fractures are correctly oriented according to equation (1) based on the initial orientation of σ_1. As a result of deformation on the R' fractures in the right lateral simple shear displacement field, there is an accompanying clockwise rotation of the direction of σ_1, shown in Fig. 6(f). Subsequent formation of R fractures was in accordance with the new clockwise-rotated direction of σ_1, leading to a clockwise rotation of R fractures and a decrease in the angle between the R and early stage R' fractures.

These effects are more pronounced as the delay between the R and R' fracture initiation increases. If both sets are formed together, the orientation should follow the standard Mohr–Coulomb relation of equation (1), in which case the angle between R and R' fractures will be at its maximum (it always decreases with finite rotation effects) and both fractures would be indicators of the current direction of σ_1. The mechanisms described can account for the angular orientation of the Riedel fractures, but a further important point to address is: why does the conjugate set of fractures develop at all? It would appear that with the effects of stress field rotation, conditions increasingly in favor of the initially dominant set would suppress development of the conjugate. The reason is shown to be the effect of boundary conditions and kinematics.

Returning to the model shown in Fig. 6(a), in which R fractures initially dominated, it might be expected that further rotation of the stress field in a counterclockwise direction would lead to late forming R fractures being oriented in the Y direction (Fig. 4). However, as relative displacement along the initially dominant fractures takes place, steps at the end of the fractures form and indent into the surrounding softer annulus. Indentation generates increasing resistance from the annulus material until fracturing along the conjugate direction becomes more favorable. Detailed examination of stress conditions in these models showed that mean stress levels near the tips of the initially dominant fracture set increased with deformation, increasing resistance of the fractures to shear displacement. The increasing stability eventually suppressed further growth of the dominant set in favor of the conjugate set. This pressure build-up was a direct consequence of the nature of the boundary conditions and another example of kinematic hardening.

The models showed that boundary conditions, in addition to stress field orientation, have a strong influence on the formation and evolution of fractures. In simple shear, both conjugate fractures develop at small post-peak strains, but through various influences, one set or the other becomes dominant. Stress field rotations associated with the dominant set suppress development of the other set. There is evidence from our models that R fractures occur most easily in simple shear, but only minor anisotropies in initial conditions could favor R' fractures. Once one set becomes dominant, the other set will only form if boundary conditions limit development of the initially dominant set.

Rotation of the stress field is a key element in the occurrence of all of the these effects. It is directly related to the boundary conditions and the strength of the material in the shear bands. Changes in stress field orientation as a result of fault strength and local changes in the stress field have been discussed to some extent in the literature (e.g. Zoback *et al.*, 1987; Zoback, 1992). Later, numerical models that were used to study the relationship between fault strength, stress field orientation and boundary conditions are described.

Combined simple and pure shear: fracture patterns

Figure 7 summarizes fracture patterns resulting from models deformed in simple shear, combinations of simple and pure shear, and pure shear alone. Convergence angle is used to express the ratio of simple to pure shear, as defined in Fig. 2. In all models, gridpoint locations were randomized, Young's modulus values were varied randomly, and except for the cases of 0°, 20° and 90° convergence, the grid alignment was not rotated to coincide with the initial σ_1 orientation.

Both R and R' fractures occur throughout the range of boundary deformation, although the proportions of each set vary. The orientation of the fractures, in general, follows the trend expected on the basis of equation (1) together with the initial orientation of the stress field, equation (2). However, the same effects of stress field rotation as noted in the models deformed in simple shear also occurred in these models.

A number of realizations for each convergence angle were simulated and the particular fracture patterns shown in Fig. 8 were not unique. The patterns showed sensitivity to initial conditions and to the evolutionary sequence. It had been thought that with decreasing proportions of simple shear compared to pure shear, and hence less rotation, both R and R' fractures would form with less favoring of one set or the other. This was not the case. Even for pure shear deformation ($\alpha = 90°$), there was unequal development of the conjugate fractures and their orientation was not symmetrical about the initial major principal stress direction (vertical in this case). At the instant of failure, both conjugate fractures theoretically have equal probability of forming. However, even with small

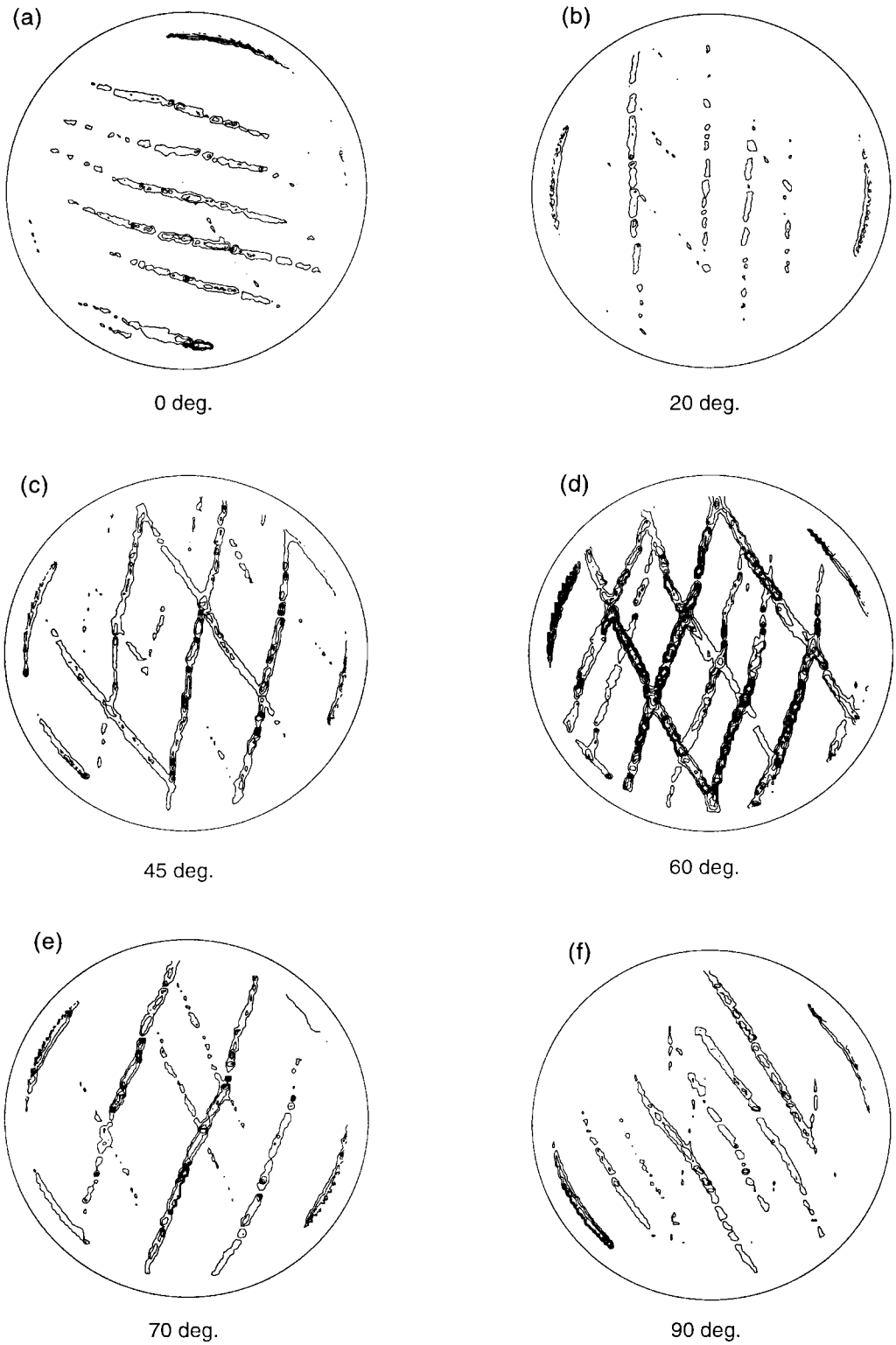

Fig. 7. Fracture patterns caused by deformation at different convergence angles. 0° convergence represents simple shear and 90° convergence is pure shear.

increments of finite strain, various factors may favor development of one set. Although we have not isolated all of the causes of this effect or their contributions, it is safe to say that kinematics and material (strength) fabric must be among the most significant factors.

Combined simple and pure shear: kinematics

The evolutionary nature of R and R' fractures significantly affects the shape of the essentially rigid block domains that form between fractures. Patterns of dis-

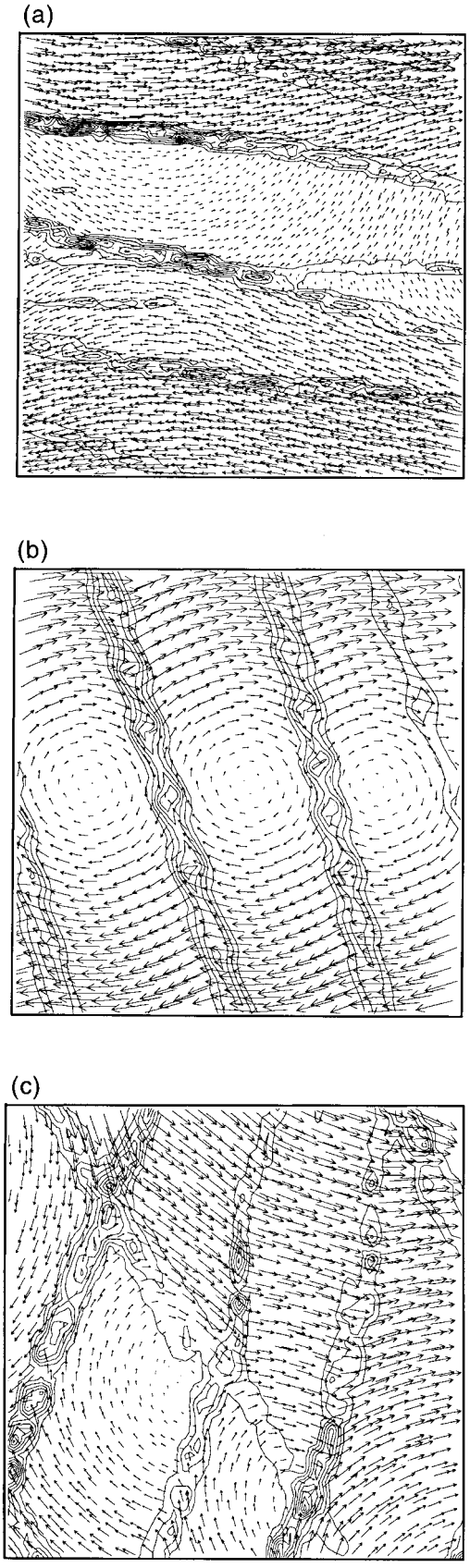

Fig. 8. Details of three models illustrating block kinematics formed by different fracture patterns. Each figure shows shear localizations that define block boundaries and total displacement vectors. (a) R fractures are dominant; (b) R' fractures are dominant; and (c) contains both R and R' fractures.

placement and velocity fields in the models provide insight into block kinematics. Boundary condition effects sometimes changed the dominant mode of fracture development causing changes in the kinematics with increasing strain. The following results, therefore, are for specific fracture geometries at particular instants in time.

Three predominant block geometries formed in the models. Blocks formed by either R or R' fractures lead initially to long thin blocks. With equally developed R and R' fractures, diamond shaped blocks formed, and with unequal R and R' development, the diamond shaped blocks became more elongated. These geometries are shown in Fig. 8, which show portions of the models with displacement vectors superimposed on shear zones.

The kinematics of an R-dominant fracture system is shown in Fig. 8(a). R fractures are rotated sub-parallel to the direction of simple shear displacement on the boundary, resulting in a system of strike-slip fractures. Displacement on these fractures is in the same sense as the direction of simple shear displacement. If the fracture system is closely aligned to the direction of the driving boundary displacement (as in this case for simple shear), there is little or no apparent rotation of the blocks. Any misalignment of the R orientation relative to the direction of simple shear leads to a progressive drop in the normal component of stress across fractures.

If R' fractures dominate, a completely different displacement field is generated (Fig. 8b). This pattern was found to be characteristic of models undergoing simple shear or simple shear with small proportions of pure shear displacement. The blocks are at a high angle relative to the external displacement field, and blocks experience both rotation and strike-slip displacement. The sense of strike-slip in these systems is opposite to the direction of external displacement.

Systems in which both R and R' fractures occur exhibit elements of the two modes described above. Figure 8(c) is such an example taken from the 60° convergence angle model. Depending on the proximity of the blocks to the model boundaries, fractures shear in either a left or right-lateral sense. Block rotation effects are distinctly non-uniform throughout the model. Near the center of the model, rotation tends to be about pivot points near block corners. Block rotation effects diminished away from the central region. This is not necessarily a general rule, but highlights how boundary conditions and block location are important in controlling block kinematics. Blocks also move relative to each other, offsetting the contacts of block corners. The kinematics of systems with both R and R' fractures is significantly more complex than in systems with only one set dominant.

Combined simple and pure shear: stress field

It has been shown how there is a general rotation of the stress field outside of shear zones, and a reduction in magnitude plus a large rotation of the stress field within shear zones. Here further details of the stress field outside of shear zones are described. Figure 9(a) shows stress tensors in the central region of a 70° convergence angle model. The coherent lines of re-oriented lower magnitude stress identify the location of shear zones. The stress field had a relatively consistent orientation within domains defined by the shear zones. In models with a high density of shear zones, the overall uniformity of the stress field was greatly reduced, but in moderately fractured systems, or those in which the amount of post-failure material softening was small, the initial stress field uniformity was largely preserved.

Changes in stress field orientation and characteristics of the induced stress field are additional useful indicators of stress field behavior. Figure 9(b), covering the same area shown in Fig. 9(a), shows the amount of rotation from the initial orientation as a result of fracturing. Clockwise rotation is positive. The stress field within intact blocks underwent a rotation generally less than 10°, whereas inside shear zones the rotation was in excess of $\pm 30°$. For the same region of the model, Fig. 9(c) shows stress change as a result of fracturing. Within shear zones, there was a tensile stress change (unloading).

The stress field within blocks formed by shear zones depended largely on their geometry and kinematics. In the example shown, the diamond shaped blocks acted as interconnected wedges with some vertices being compressed by adjacent block sides whereas others experienced very little stress change or minor unloading. Stress changes in the interior of blocks was generally more uniform than close to block vertices.

Combined simple and pure shear: fracture strength

The observations made in the previous sections are specific to the particular models described and should not be generalized without some qualification. Firstly, a specific post-failure constitutive model was assumed, and the strength loss of fractures strongly influences the stress field within the surrounding blocks. Within shear zones, rapid loss of cohesion was assumed but friction was not diminished. Since the initial friction angle was assumed to be quite high, the inter-block strength across fractures was still relatively high, thus preserving the orientation of the intra-block stress field.

Not a great deal is known about fault strength because of the impossibility of direct measurement. Measurement of the stress field around faults or analysis of seismic records from known fault movements is useful in this regard. In contrast with these difficulties in real systems, physical properties specified in numerical models can be easily varied.

To observe the effects of particular parameters on system behavior, it is useful to model extreme cases. While these models may not be realistic, they unambiguously highlight the effects of specific parameters. To observe the effect of fracture strength, therefore, a very low post-failure strength was assigned to the material in the model. For comparison purposes, reference is made to the model with 70° convergence angle [see Fig. 7(e) for fracture pattern with no friction soft-

(a)

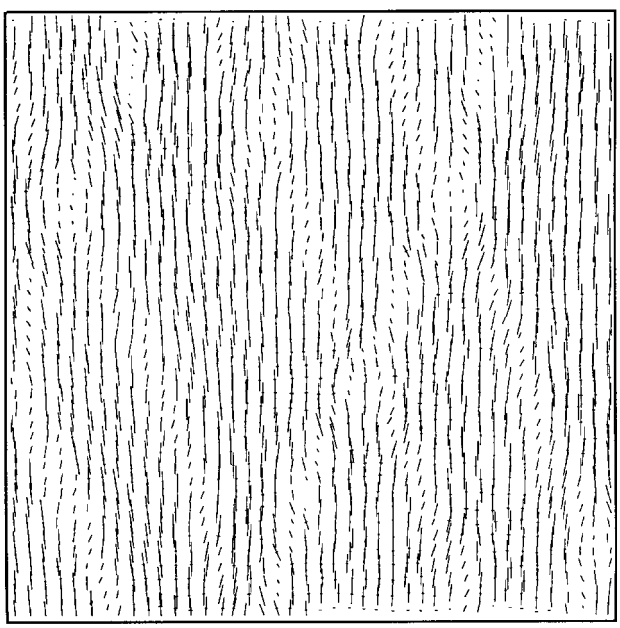

Fig. 9a—*Caption opposite*

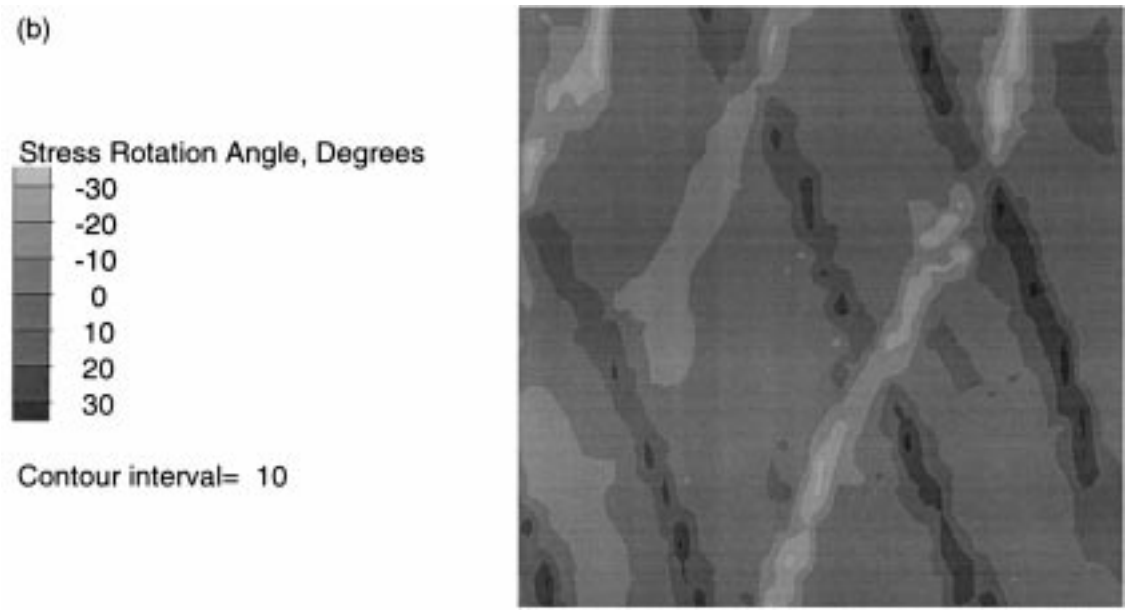

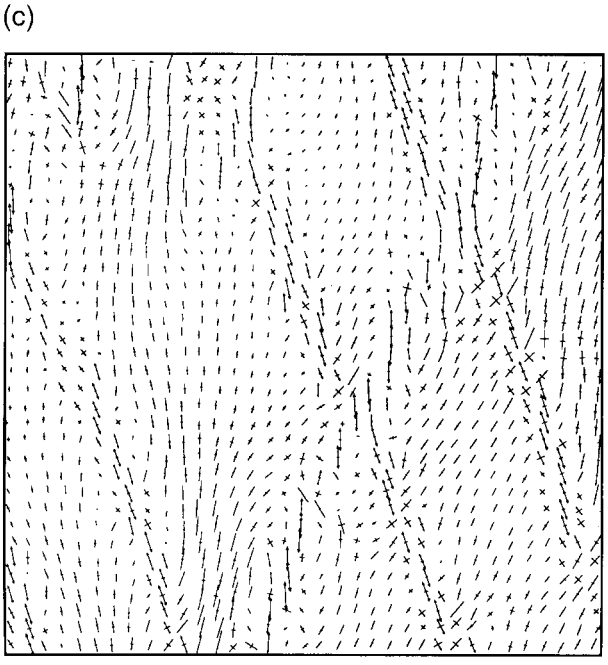

Fig. 9. Detail of 70° convergence angle model showing: (a) tensors of total stress field; (b) rotation from initial orientation; and (c) stress change. Tensile stress changes are depicted as arrows in the stress tensors of (c).

ening, and Fig. 9(a) for the stress field]. The new model was identical to the previous one except that upon failure, the material friction angle was specified to soften from 55° to 5° after a plastic strain of 0.01. Cohesion was assumed to be completely lost over the same strain interval. This is a fairly rapid and large drop in strength (see Hoek and Bray, 1977, for typical soil and rock friction angles).

Figure 10(a) shows the fracture pattern that developed over approximately the same interval of strain as the model shown in Fig. 7(e). The number of fractures is much smaller than in the higher strength case, but the orientation is approximately the same. The displacement field in the model showed that the blocks formed by the fractures were essentially rigid. An examination of the stress field in the system provides the greatest insight into the effect of rapid and large strength loss. Figure 10(b) shows the stress field and fracture locations in the central region of the model. The stress field is highly non-uniform compared to the higher strength case (Fig. 9a). Significant changes in both magnitude and orientation of the stress field have taken place.

In terms of the mechanics of this system, low strength fractures cannot sustain high shear stresses. Reduction in shear stresses on fractures takes place

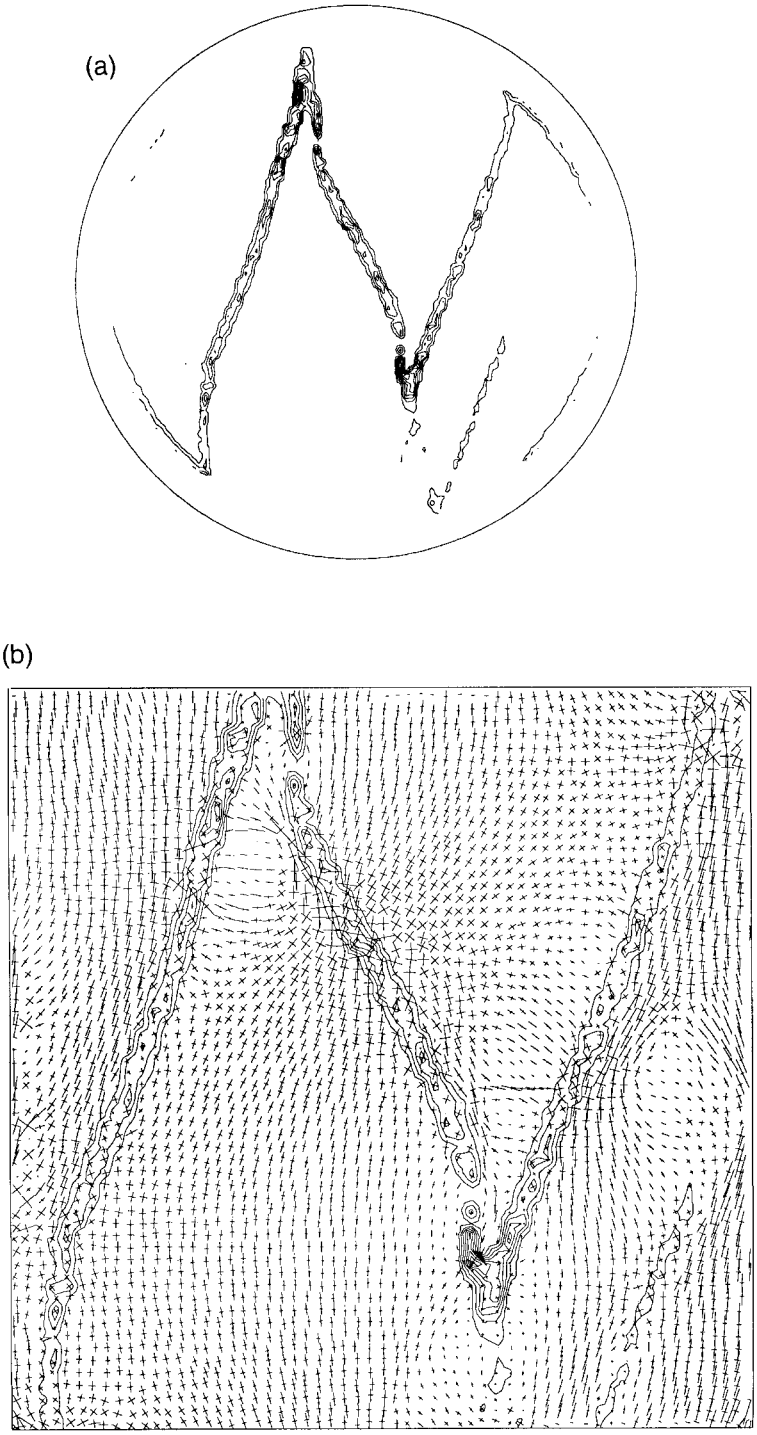

Fig. 10. Effect of rapid strain softening of fractures on stress field, 70° convergence angle model. (a) Fracture pattern; and (b) detail of stress field.

through slip. However, because of boundary constraints on large displacements, the amount of slip that could occur is limited. This is the same kinematic hardening effect as noted previously. As a result, the flow of stress within the model was complex, and was accommodated by a number of highly compressive stress bridges across fractures. Such a bridge is shown in Fig. 10(b). The major principal stress is oriented at a high angle to the fractures in these locations and at a low angle elsewhere. Where the principal axes are oblique to fractures the magnitudes of the principal stresses are similar, implying low shear stress levels. The formation of stress bridges results in large changes in the orientation and magnitude of the stress field over the length of the fractures.

Since the initial fractures caused a large distortion of the stress field, subsequent formation of linear fractures was suppressed. Conversely, the occurrence of

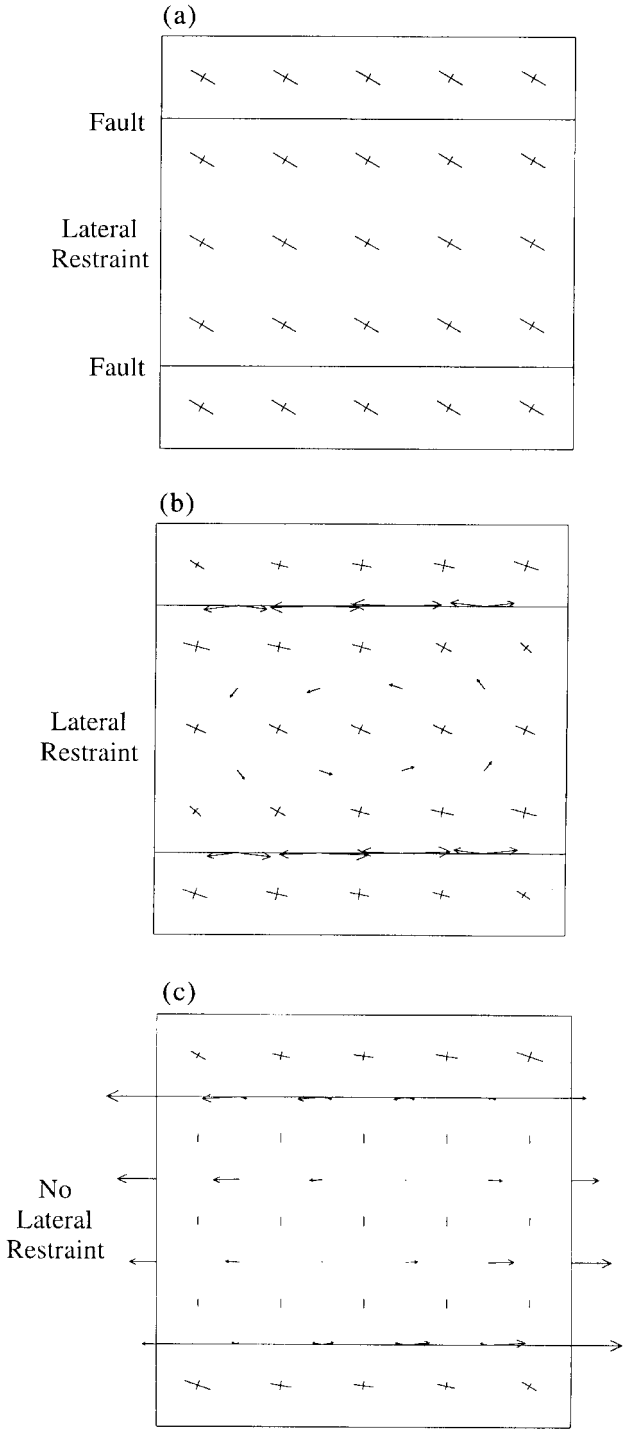

Fig. 11. Simple model illustrating effects of both boundary condition and fault strength on orientation of stress field. Model (a) is initially in equilibrium with rigid confinement and welded faults; (b) has fault strength reduced to zero, displacement vectors shown in addition to stress tensors; and (c) has lateral confinement released.

many nearby linear fracture zones would indicate that strength loss is small. Models with more modest loss of strength, with softening of friction angle to a more realistic value of 30°, showed similar consistency of the intra-block stress field as the non-friction softening models.

To illustrate the interaction of stress field, fault strength and boundary conditions, a simple model was constructed (Fig. 11). The model had two initially welded faults (Fig. 11a), and the axis of the major principal stress was inclined at 30° to the faults. Displacement on all boundary points was rigidly restrained and the model was in stress equilibrium. This state represented faults prior to failure or any strength loss. By reducing the strength of the faults to zero, slip occurred (Fig. 11b). However, since the boundaries of the model were restrained, only partial slip occurred. The direction of displacement in the central section of the model between the faults was counterclockwise, consistent with the release of positive shear stresses. This behavior is a form of elastic 'unwinding'. Because shear stresses had been completely eliminated across the fault, the stress field in the adjacent zones rotated and the principal stress magnitudes changed. Finally, by removing the lateral restraint from the central section of the model (Fig. 11c), lateral stresses were completely relaxed by lateral displacements. The final stress field was uniaxial, oriented at right angles to the strike of the fault.

The behavior of the stress field shown in Fig. 11(b) is relevant to the models of fracture evolution described here in that most models had some form of boundary restraint. In all models, strength softening was used. If there is kinematic restraint of slip on fractures or faults, the stress field will not rotate as much as it would if the system were unrestrained. Therefore, interpretation of stress field orientation in terms of fault strength can be complex.

Stability of fracture patterns as a result of changes in boundary condition

The modeling results showed that the orientation of new fractures can change with increasing boundary deformation as a result of stress field rotations. A related problem is the stability of a fracture pattern with changes in boundary condition. Stability in this context refers to whether or not the initial mode of fracturing and deformation is preserved after a change in boundary condition. This could occur, for example, because of a change in plate motion. Using equation (2), it can be shown that the orientation of the major principal stress changes most rapidly as boundary conditions change from simple shear to oblique deformation. In addition, if predominantly R oriented fractures occur in the simple shear model, additional amounts of pure shear result in increased normal stress on the fractures. This would increase their resistance to shear displacement and tend to inhibit further growth. On this basis, the effects of changes in loading condition were expected to be most noticeable for the case of an R dominant system in simple shear to which a component of pure shear is added.

In the model, fractures were initially allowed to develop as a result of right lateral simple shear. The randomly distorted but unrotated grid resulted in pre-

dominantly R oriented fracture growth similar to that shown in Fig. 7(a). After 5000 steps a component of pure shear was added to simulate a 20° convergence angle and the simulation continued up to 30,000 steps. It was found that the pattern of fracture formation was unaffected as illustrated by a history of the average orientation of the major principal stress in the model (Fig. 12). At the 5000 step point in the simulation there was no apparent change in the slope of the curve (Fig. 12) to indicate that the boundary condition had changed.

The existing fracture pattern persists because the internal stress field is unaffected at the instant of change in boundary condition. The stress field remains compatible with the initial boundary displacement path and fracture pattern development. The existing fractures also alter the material to give it anisotropic strength, favoring slip on existing fractures as opposed to formation of new fractures at a slightly different angle. The stability of this fracture pattern would have been increased if the strain softening of the fractures had been greater.

The issue of new fracture formation or continued slip on existing fractures, as presented here, should be contrasted with the problem of calculating the stability of a fault plane under the influence of an arbitrary stress field. In the latter case, the initial stress field would have to be replaced by one compatible with the new direction of loading. For this to occur, the region would have to experience a relaxation of boundary restraint or a time-dependent dissipation of the internal stress field prior to generation of the new stress field consistent with the second stage of loading.

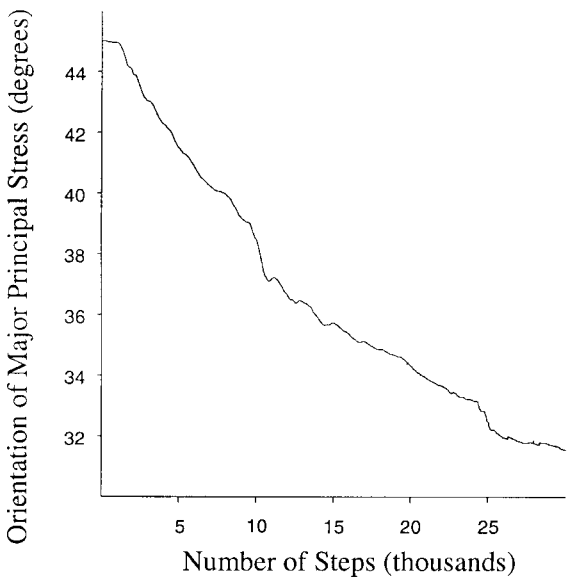

Fig. 12. Orientation of major principal stress in R dominant right-lateral shear model. Up to 5000 steps the deformation was simple shear and thereafter set to 20° convergence angle. The record of stress field rotation shows no effect of the change in boundary condition.

A simpler example of this problem is the stability analysis of a single fault plane in a biaxial or two-dimensional stress field (Jaeger and Cook, 1976; Hoek and Brown, 1980). This approach has been applied to the stability of faults separating rotating blocks in a stationary stress field (Nur *et al.*, 1989). Conceptually, this analysis is applicable to the stability of fracture systems caused by changing boundary conditions, except that with confined boundaries, there is a more complex relationship between changes in the boundary loading and changes in the stress field within the region influenced. Our results show that boundary restraint can have a significant effect on preserving the original stress field such that fault stability cannot be assessed simply on the basis of assuming a new stress field orientation.

CONCLUSIONS

Continuum# models were used to generate localizations of shear failure, or fractures. Both R and R' oriented fractures, defined by Mohr–Coulomb angular relationships to the major principal stress, were readily reproduced, followed by Y oriented fractures at larger strains. Strength loss in shear localizations requires that shear stress levels be reduced, leading to a reduction in magnitude and rotation of the principal stresses. With increasing strength loss, both magnitude and orientation of the stress field outside of the shear zones become affected. New fractures forming in this rotated stress field are rotated relative to the orientation of the initial fractures. Y oriented fractures were shown to be consistent with Mohr–Coulomb shear failure provided the stress field rotation is accounted for.

Both the strength of the shear zones and the boundary conditions of the region are important in determining the behavior of the stress field outside of shear zones. Fracture development in a region undergoing deformation may vary significantly depending on whether the boundaries are confined or unconfined. Boundary conditions or material fabric anisotropies may lead to either R or R' fractures becoming dominant. Depending on the sense of boundary displacement and whether R or R' fractures dominate, the stress field may rotate clockwise or counterclockwise. As deformation progresses, even constant boundary conditions could lead to a change in which fracture set dominates as a result of a process referred to as kinematic hardening.

The shape of blocks formed by Riedel fractures depends on whether one set is dominant or both are present. The orientation and location of blocks relative to the driving displacement affects the kinematics of block rotation and translation.

Existing fractures accommodate boundary displacement by sporadic displacement, i.e. fractures are not all active at the same time. Activity appeared to alternate between fractures, distributing strain over time.

Interpreted in terms of seismic activity, many faults in driven systems such as those modeled may appear to be inactive in short time windows although they may be equally active in accommodating displacement in the longer term. In such circumstances, short-term seismic activity may not be a good discriminator of fault activity.

Variations in magnitude and orientation of the principal stresses in a fractured rock mass are a natural consequence of the differences in strength between intact rock and discontinuity surfaces. Domains of relatively uniform stress fields can be expected to coincide with structural domains. This link is useful to identify when interpreting stress measurements.

Stress measurements carried out within a single domain defined by shear fractures or faults would be expected to show similar orientations of σ_1, and this orientation would be similar to the orientation found in other domains provided the intervening fractures do not have low strength. Close to fractures or faults, larger variations would be expected. Data from the World Stress Map Project (Zoback, 1992) shows a reasonable degree of coherency in the orientation of the horizontal principal stress on a regional basis. This is noteworthy, considering that major structural features exist on regional scales but apparently do not significantly distort the overall trend of regional stress fields. A study of stress measurements in the Mediterranean region (Rebaï *et al*., 1992) concluded that stress domains are defined by structures on different scales, i.e. large structures define large domains of stress, but within these domains, smaller domains of stress may be defined by sub-structures. This theme is consistent with the results of the numerical models.

Changes in boundary deformation do not immediately lead to changes in the internal stress field of a region. Boundary restraint can preserve the initial stress field and existing fractures result in a weak fabric to the rock mass. These factors may favor continued deformation of existing fractures as opposed to generation of new fractures consistent with the new loading conditions.

Acknowledgements—Part of this work was carried out for the *Projecto Geodinámico*, sponsored by CODELCO-Chile, Division El Teniente. Their support of this work and permission to publish is gratefully acknowledged. Basil Tikoff, Rice University, is thanked for his review and helpful suggestions, as is Christian Teyssier, University of Minnesota. Referees Sandy Steacy and Alison Ord are also thanked for their reviews, which helped to improve the paper.

REFERENCES

Atkinson, J. H. and Bransby, P. L. (1978) *The Mechanics of Soils*. McGraw Hill, London, UK.

Bartlett, W. M., Friedman, M. and Logan, J. M. (1981) Experimental folding and faulting in rocks under confining pressure. Part IX. Wrench faults in limestone layers. *Tectonophysics* **79,** 255–277.

Bažant, Z. P. (1992) *Fracture Mechanics of Concrete Structures*. Elsevier Science, London.

Braun, J. (1994) Three-dimensional numerical simulations of crustal-scale wrenching using a non-linear failure criterion. *Journal of Structural Geology* **16,** 1173–1186.

Cundall, P. A. (1989) Numerical experiments on localization in frictional materials. *Ingenieur-Archiv* **59,** 148–159.

Cundall, P. A. (1990) Numerical modeling of jointed and faulted rock. In *Mechanics of Jointed and Faulted Rock*, ed. H. P. Rossmanith, pp. 11–18. Balkema, Rotterdam.

Gamond, J. F. (1983) Displacement features associated with fault zones: a comparison between observed examples and experimental models. *Journal of Structural Geology* **5,** 33–45.

Hobbs, B. E. and Ord, A. (1989) Numerical simulation of shear band formation in a frictional–dilational material. *Ingenieur-Archiv* **59,** 209–220.

Hoek, E. and Bray, J. (1977) *Rock Slope Engineering*. The Institution of Mining and Metallurgy, London.

Hoek, E. and Brown, E. T. (1980) *Underground Excavations in Rock*. The Institution of Mining and Metallurgy, London.

Itasca Consulting Group Inc. (1995) *FLAC (Fast Lagrangian Analysis of Continua), version 3.3*. ICG, Minneapolis.

Jaeger, J. C. and Cook, N. G. W. (1976) *Fundamentals of Rock Mechanics*. Chapman and Hall, London.

Naylor, M. A., Mandl, G. and Sijpesteijn, C. H. K. (1986) Fault geometries in basement-induced wrench faulting under different initial states of stress. *Journal of Structural Geology* **8,** 737–752.

Nur, A., Ron, H. and Scotti, O. (1989) Kinematics and mechanics of tectonic block rotations. In *Slow Deformation and Transmission of Stress in the Earth. Geophysical Monograph* **49,** ed. S. V. Cohen and P. Vanicek, pp. 31–46. American Geophysical Union, Washington.

Olson, J. E. and Pollard, D. D. (1991) The initiation and growth of en échelon veins. *Journal of Structural Geology* **13,** 595–608.

Rebaï, S., Philip, H. and Taboada, A. (1992) Modern tectonic stress field in the Mediterranean region; evidence for variation in stress directions at different scales. *Journal of Geophysical Research* **109,** 1–35.

Riedel, W. (1929) Zur mechanik geologisher brucherscheinungen. *Zentralblatt für Mineralogie, Geologie und Paleontologie* **B,** 354–368 (Abhandlung).

Rudnicki, J. W. and Rice, J. R. (1975) Conditions for the localization of the deformation in pressure-sensitive dilatant materials. *Journal of Mechanics and Physics of Solids* **23,** 371–394.

Sylvester, A. G. (1988) Strike-slip faults. *Geological Society of America Bulletin* **100,** 1666–1703.

Tchalenko, J. S. (1970) Similarities between shear zones of different magnitudes. *Geological Society of America Bulletin* **81,** 1625–1640.

Tchalenko, J. S. and Ambraseys, N. N. (1970) Structural analysis of the Dasht-e Bayaz (Iran) earthquake fractures. *Geological Society of America Bulletin* **81,** 41–60.

Vermeer, P. A. (1982) A simple shear-band analysis using compliances. In *Deformation and Failure of Granular Materials*, eds P. A. Vermeer and H. J. Luger, pp. 493–499. Balkema, Rotterdam.

Vermeer, P. A. (1990) The orientation of shear bands in biaxial tests. *Geotechnique* **40,** 223–236.

Zoback, M. L. (1992) First- and second-order patterns of stress in the lithosphere; the World Stress Map Project. *Journal of Geophysical Research* **97**(B8), 11,703–11,728.

Zoback, M. D., Zoback, M. L., Mount, V. S., Suppe, J., Eaton, J. P., Healey, J. H., Oppenheimer, D., Reasenberg, P., Jones, L., Raleigh, C. B., Wong, I. G., Scotti, O. and Wentworth, C. (1987) New evidence on the state of stress of the San Andreas Fault system. *Science* **238,** 1105–1111.